THESIS FOR THE DEGREE OF LICENTIATE OF ENGINEERING

Manganese Combined Oxides as Oxygen Carriers for Chemical-Looping Combustion

MALIN KÄLLÉN

Department of Energy and Environment

CHALMERS UNIVERSITY OF TECHNOLOGY

Gothenburg, Sweden 2014

Manganese Combined Oxides as Oxygen Carriers for Chemical-Looping Combustion

MALIN KÄLLÉN

Department of Energy and Environment
Chalmers University of Technology
SE-412 96 Gothenburg
Sweden
Telephone + 46 (0)31-772 1000

Reproservice
Gothenburg, Sweden 2014

Manganese Combined Oxides as Oxygen Carriers for Chemical-Looping Combustion

MALIN KÄLLÉN
Division of Energy Technology
Department of Energy and Environment
Chalmers University of Technology

Abstract

The global emissions of greenhouse gases are increasing and the development of mitigation measures is becoming more important. One of the alternatives proposed is carbon capture and storage, where the carbon dioxide emitted from large point sources is captured, compressed and stored in underground storage sites. Many of the largest point sources of carbon dioxide are power plants fuelled by fossil fuels. There are several technologies for adapting the combustion process to capture carbon dioxide. Chemical-looping combustion is one such option and has the advantage of keeping the fuel and the combustion air apart, thus avoiding energy consuming carbon dioxide-nitrogen separation. This is achieved by transferring oxygen from the air to the fuel by a cyclic oxidation and reduction of a solid metal oxide. The oxygen-carrying material needs to meet a number of requirements in order to achieve an efficient combustion process.

Manganese oxides have promising properties as oxygen-carrier material and these can be further improved by combining the manganese with for example iron, silica and calcium. Chemical-looping combustion is mainly developed as a technology for fluidised-bed combustion with the oxygen carrier present as the bed material in the form of small particles. To perform well in a circulating fluidised bed the oxygen carrier needs to be mechanically stable as well as have good reactivity with the fuel. During the development of manganese combined oxides, materials with such properties have been identified.

The work presented in this thesis examines the performance of manganese combined oxides as oxygen carriers in interconnected fluidised beds with continuous circulation. The operation has been carried out in two reactor systems with gaseous fuels, in which the properties of the materials have been evaluated. It has been shown that full conversion of the fuel can be achieved during chemical-looping combustion in a 10 kW_{th} reactor unit with a calcium manganite of perovskite structure as oxygen carrier. Furthermore, combined oxides of iron-manganese-silica and manganese-silica have been examined in a 300 W_{th} reactor unit. High fuel conversion was achieved with both combined oxides systems, but the mechanical stability of these materials was not satisfactory. It was found that the mechanical stability of combined oxides of manganese-silica could be improved by adding titania to the material. Future work would include further investigation regarding the effect of the material composition on the performance.

Keywords: carbon capture, chemical-looping, combined oxide, manganese oxide

List of Publications

This thesis is based on the work presented in the following publications:

Paper I Källén M, Rydén M, Dueso C, Mattisson T, Lyngfelt A. $CaMn_{0.9}Mg_{0.1}O_{3-\delta}$ as oxygen carrier in a gas-fired 10 kW_{th} chemical-looping combustion unit. Industrial and Engineering Chemistry Research. 2013;52:6923-32.

Paper II Källén M, Hallberg P, Rydén M, Mattisson T, Lyngfelt A. Combined oxides of iron, manganese and silica as oxygen carriers for chemical-looping combustion. Fuel Processing Technology. 2014;124:87-96.

Paper III Källén M, Rydén M, Lyngfelt A, Mattisson T. Chemical-Looping Using Combined Iron/Manganese/Silica Oxygen Carriers. In: Proceedings of the 3rd International Conference on Chemical Looping. Gothenburg, Sweden, 2014.

Paper IV Källén M, Rydén M, Mattisson T, Lyngfelt A. Operation with combined oxides of manganese and silica as oxygen carriers in a 300 W_{th} chemical-looping combustion unit. In: Proceedings of the 12th International Conference on Greenhouse Gas Technologies. Austin, USA. 2014.

Contribution report:

Paper I: principal author, responsible for part of the experimental work and for a majority of the data evaluation.

Paper II, III and IV: principal author, responsible for experimental work and data evaluation.

Related publications not included in this thesis:

- Rydén M, Källén M, Jing D, Hedayati A, Mattisson T, Lyngfelt A. $(Fe_{1-x}Mn_x)Ti_yO_3$ based oxygen carriers for chemical-looping combustion and chemical-looping with oxygen uncoupling. 7th Trondheim Conference on CO_2 Capture, Transport and Storage, TCCS 2013. Trondheim: Elsevier Ltd; 2013. p. 85-98.

- Rydén M, Jing D, Källén M, Leion H, Lyngfelt A, Mattisson T. CuO-based oxygen-carrier particles for chemical-looping with oxygen uncoupling - Experiments in batch reactor and in continuous operation. Industrial and Engineering Chemistry Research. 2014;53:6255-67.

- Hallberg P, Källén M, Jing D, Snijkers F, Van Noyen J, Rydén M, Lyngfelt A. Experimental investigation of $CaMnO_{3-\delta}$ based oxygen carriers used in continuous chemical-looping combustion. International Journal of Chemical Engineering. 2014;2014.

Acknowledgement

First of all I want to thank my supervisors Anders Lyngfelt and Magnus Rydén for always taking the time to discuss and answer my questions. Anders, thank you for your enthusiasm which always makes me want to improve and know more. Magnus, thank you for your relaxed attitude which always makes me calm down when I am stressed over things not going so well. I also want to thank Tobias Mattisson for always acting as my supervisor in practice, although not being it in theory. I would also like to take the opportunity to thank Henrik Leion for introducing me to the fascinating world of chemical-looping combustion back in 2009 and for finally making me understand that I wanted to become a PhD student after all.

Louise, I want to thank you for being a great friend throughout our studies at Chalmers. We have shared all the joy and suffering during the education and I really appreciate to have you as my roommate now that we both decided to stay at Chalmers for another five years.

A large part of this work has been carried out in the CLC-lab, and I am really grateful to Patrick, Peter, Matthias, Calle and Jesper for contributing to a cheerful working atmosphere. Even though we sometimes have our disagreements (mostly about cleaning), it is most often a joy to work in the lab thanks to you all. I also want to thank Ulf and Rustan for all practical help and for cheering me up when I have a bad experimental day.

I am also very grateful to all my other colleagues for creating a great working atmosphere. I want to thank my fellow chemical-loopers Dazheng, Golnar, Sebastian, Volkmar, Martin, Pavleta, Mehdi, Pontus and Dongmei as well as all the people at Energy Technology.

My greatest thankfulness goes to my family and my friends. Thank you for always being there and supporting me. A special thanks to my parents who taught me to be curious and that I should always do my best. Finally and foremost, Hasse, it is your love and support that keeps me going and I am so grateful for sharing life with you.

Table of Contents

1. Introduction

The increasing emission of greenhouse gases is one of the largest challenges facing humankind today. The accumulation of these gases in the atmosphere will cause climate changes associated with an increased average global temperature. [1] The changes in the climate will inevitably harm ecosystems as well as living conditions for humans in many parts of the world. [2] The largest average increase in greenhouse gas emissions ever was observed in the decade 2000-2010 when the emissions rose with 2.2%/year in average. A substantial part of the emissions originates from the production of electricity and heat which gives rise to 25% of the total emissions of greenhouse gases. The production of electricity and heat is mainly fuelled by fossil fuels. [3]

Renewable energy sources like solar and wind power are often viewed as the solution to the energy supply problem. However, even though the implementation of these technologies has developed very fast, it will take a rather long time for them to substitute fossil fuels completely. Carbon capture and storage (CCS) has been proposed as a bridging technology between today's energy production and a renewable energy system. CCS includes the capture of carbon dioxide from point sources such as power plants, compression, transportation and finally deposition at a storage site. CCS could also make it possible to achieve negative greenhouse gas emissions, if it is used for a process fuelled by biomass.

The capture of carbon dioxide will most certainly be the most costly part of the CCS chain. A number of technologies for carbon dioxide capture have been developed and they can be classified in three categories: pre-combustion, post-combustion and oxy-fuel combustion. In pre-combustion capture the fuel is reformed to carbon monoxide and hydrogen. The carbon monoxide is then reacted with steam to form carbon dioxide and more hydrogen. A gas separation unit is necessary to separate the carbon dioxide from the hydrogen, which can be used as a carbon free fuel. In post-combustion capture the carbon dioxide is separated from the flue gases after combustion in a gas separation unit. In oxy-fuel combustion the fuel is burnt in oxygen and recycled flue gases. An air separation unit is needed to produce pure oxygen from air. [4]

All these technologies would require gas-gas separation which is costly and very energy intensive. Another capture technology proposed called chemical-looping combustion avoids this separation and may therefore capture carbon dioxide at a much lower cost. [5]

1.1. Chemical-Looping Combustion

The technology of chemical-looping combustion is based on the cyclic oxidation and reduction of a metal oxide. The combustion is carried out in two steps in two separate reactor vessels. The first one is commonly called the air reactor (AR) and here the metal oxide is oxidised by a stream of air. The second reactor is called the fuel reactor (FR) and here the metal oxide is reduced and the

fuel is oxidised as these react. The metal oxide is therefore referred to as an oxygen carrier. The combustion scheme is illustrated in Figure 1.

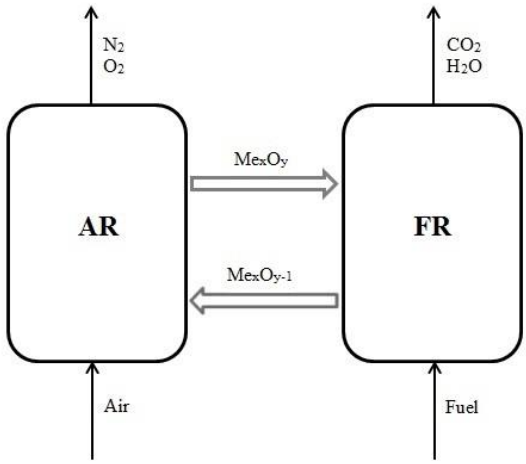

Figure 1. Basic principle of the combustion scheme chemical-looping combustion.

The heat of combustion will be identical to normal combustion in air. This can be shown by adding up the two reaction steps shown below:

$$Me_xO_{y-1} + \frac{1}{2}O_2 \rightarrow Me_xO_y \quad (1)$$

$$(2n+m)Me_xO_y + C_nH_{2m} \rightarrow (2n+m)Me_xO_{y-1} + mH_2O + nCO_2 \quad (2)$$

As is seen in the overall reactions above, the metal oxide is often not reduced fully to the metal state, although this is a possibility and depends on the system used. The fuel combustion in chemical-looping combustion will differ depending on if it is a gaseous fuel or a solid fuel which is being burnt. In combustion of gaseous fuels the fuel can react directly with the oxygen carrier in a gas-solid reaction. In combustion of a solid fuel, the volatiles will first be released in gaseous form and they can react directly with the oxygen carrier. The remaining char needs to be gasified first to produce a gas which may react with the oxygen carrier in a gas-solid reaction. The direct solid-solid reaction between the char and the oxygen carrier would be a very slow and inefficient reaction route.

Char gasification is a rather slow reaction compared to the other reactions in the combustion scheme and would therefore be the rate limiting factor for the char conversion. The selection of oxygen-carrier material offers a way to get around this problem. Some metal oxides are capable of releasing oxygen in gas phase at the temperatures which are relevant for fuel combustion according to:

$$Me_xO_y \rightarrow Me_xO_{y-1} + \frac{1}{2}O_2 \quad (3)$$

Some or all of the char can then react directly with the released gaseous oxygen and will not need to be gasified. This combustion scheme is referred to as chemical-looping with oxygen uncoupling (CLOU). [6] Chemical-looping with oxygen uncoupling can also be advantageous in combustion of gaseous fuels as it would enable a gas-gas reaction between oxygen and fuel instead of a gas-solid reaction which would be much slower. This implies that CLOU can facilitate complete combustion even though the mixing between oxygen carrier and fuel is not sufficient.

A common way to realise chemical-looping combustion is by using two interconnected fluidised bed reactors. The oxygen carrier has then the form of small particles of a suitable size range. By using this method, knowledge and experience of combustion in circulating fluidised bed boilers can be used. The air reactor is a circulating fluidised bed with high gas velocities, which is needed in order to transport the particles from the bed to the fuel reactor. The fuel reactor can either be a bubbling bed with lower gas velocities or a circulating fluidised bed with an internal circulation loop. The latter is usually regarded to be more advantageous for solid fuels. Most chemical-looping pilot units in operation today uses interconnected fluidised beds as combustion method.

Chemical-looping combustion was first introduced as a technology to produce carbon dioxide in a patent application in 1954. [7] Later, the idea of using the process to capture carbon dioxide from combustion of fossil fuels was formed. [8] The proof of concept came in 2004, when Lyngfelt and Thunman [9] constructed and operated a 10 kW chemical-looping combustor for more than 100 h. The development has progressed very fast since the first studies. Today more than 700 oxygen-carrier materials have been examined worldwide and the total continuous operation now amounts to more than 4000 h in chemical-looping units ranging from 300 W to 140 kW; see recent review articles by Lyngfelt [10] and Adanez et.al. [11] for an overview.

1.2. Oxygen Carriers

The development of oxygen carrier materials is crucial for the progress of chemical-looping combustion. There are a large number of requirements for materials to be suitable as oxygen carriers. The metal oxide should be oxidised and reduced at sufficient rate at relevant temperatures and not break down due to the chemical stress. The rate of oxidation and reduction will decide the amount of material needed in each reactor vessel. The mass fraction of oxygen that the oxygen carrier is able to transfer per cycle, i.e. the oxygen transfer capacity, is another important parameter. The material should be inert towards fuel impurities such as sulphur. If the combustion is carried out in fluidised beds, the mechanical integrity is a decisive property as the gas velocities in such reactors are high and the material will follow the gas flow through cyclones. When chemical-looping is scaled up to commercial scale, large quantities of the oxygen carrier material will need to be handled. Therefore it is preferable if the material is rather cheap and neither toxic nor environmentally harmful. If the oxygen carrier will be used in chemical-looping with oxygen uncoupling, the rate of oxygen release will be a central parameter.

Oxygen-carrier materials suitable for chemical-looping combustion were identified in a thermodynamic analysis. [12] The oxides of nickel, copper, iron, manganese and cobalt were found to be feasible for chemical-looping conditions. For a long time nickel was the most used oxygen carrier and regarded as state of the art. [13, 14] However, nickel is both expensive and toxic and has a thermodynamic constraint of 99-99.5% fuel conversion, depending on temperature and pressure. The thermodynamic constraint is even worse for cobalt, where the maximum fuel conversion is 93% at relevant combustion temperatures. [15] Therefore there are very few studies with cobalt oxygen carriers. Iron oxides have been more frequently been studied as oxygen carriers for chemical-looping combustion. The reactivity is usually tolerable and the mechanical stability is regarded as good. [16]

The interest in copper oxide oxygen carriers has increased lately due to the oxygen release properties of this material. [17] Copper is reactive and gives good conversion of the fuel, but has the disadvantage of being rather expensive. The mechanical stability of copper materials is also uncertain. [18] Manganese oxide has oxygen release properties as well, but the relevant equilibrium concentrations occurs below 800°C and the reoxidation of the material is very slow at lower temperatures. [6] However, the thermodynamic properties of manganese oxides can be altered by combining the manganese with other metals. [19]

Manganese oxides have been combined with iron, silicon, calcium, nickel, magnesium and copper. [19] Combined oxides of manganese-iron, manganese-nickel and manganese-silica were operated in a batch fluidized reactor. [20] Later research has focused more on combined oxides of iron and manganese, silicon and manganese and also combined oxides of iron, manganese and silicon. These systems have the ability to release oxygen and have all shown promising results. All these materials have been examined in laboratory batch reactors. [21-23] Two materials consisting of manganese and iron have been operated continuously in a 300 W reactor system. [24] In order to examine these kinds of materials further, five combined oxides of iron, manganese and silica, Paper II and Paper III, and two combined oxides of manganese and silica, Paper IV, have been examined in continuous operation in this work.

The combined oxides of manganese and calcium can form perovskite structures which are very interesting for chemical-looping with oxygen uncoupling. The unit cell of perovskite crystal structures has the general formula $ABO_{3-\delta}$ in which A represents a larger cation and B a smaller cation. There can be more than one type of A atom or B atom as long as the radii of the atoms are very similar. The δ in the formula expresses the degree of oxygen deficiency in the structure and is zero for an ideal perovskite. The oxygen content of the structure can be increased or reduced by altering factors in the surroundings such as temperature, pressure or oxygen partial pressure. The surroundings in a chemical-looping air reactor are oxidising, while they are reducing in the fuel reactor. Therefore δ_{ar} will be smaller and δ_{fr} will be larger. The amount of oxygen available for oxidation of fuel via oxygen release can be written as (δ_{fr} - δ_{ar}):

$$CaMnO_{3-\delta ar} \leftrightarrow CaMnO_{3-\delta fr} + \tfrac{1}{2}(\delta_{fr}-\delta_{ar})\, O_2 \qquad (4)$$

The equilibrium oxygen content of calcium manganite perovskite has previously been examined outside the chemical-looping research area. [25] Perovskite oxygen carriers based on calcium manganite have been examined in a batch reactor [26, 27] as well as in continuous operation [28, 29] with promising results. This type of materials has also been studied in this work, Paper I, and is the first study of this sort of material in continuous operation at relevant industrial conditions.

Most of the operation with oxygen carriers has been carried out with synthetic materials. The production of the oxygen carrier increases the cost of the material, compared to the price of the raw materials. This may not be an issue for operation with gaseous fuels as these are quite pure and do not produce any ashes. This may however be a problem during operation with solid fuel where the oxygen carrier probably will have a lower operational lifetime. [30] This issue has caused a search for natural materials with good oxygen carrier properties. The state of art in this category is ilmenite and has been so for a couple of years. Ilmenite is an ore consisting of iron-titanium oxide and it has been operated with solid fuel in many pilot units. [31-33] Also iron and manganese ores and have more recently been examined as oxygen carriers. [34-36]

1.3. Objective of Study

In the last few years there have been some efforts on finding suitable manganese combined oxides for use in chemical-looping. However, almost all work has been conducted in small laboratory units with a very limited number of red-ox cycles. This work is the first major effort to investigate interesting manganese combined oxides in continuous operation. Hence, the objective of this research is to evaluate a number of manganese combined oxides as oxygen carriers in continuous operation, and thus more relevant conditions. The oxygen release, reactivity with fuel and mechanical stability were the key performance indicators which were assessed. The long-term aim is to find viable oxygen carrier materials for large-scale operation. A portfolio of different materials will be needed as the desired characteristics of the oxygen carrier will depend on the fuel used and in which scale the operation will run. Paper I is aimed at evaluating a material for operation with gaseous fuels and Papers II, III and IV are aimed at finding materials for operation with solid fuels.

2. Experimental

The oxygen-carrier materials produced were evaluated during fluidisation in inert atmosphere as well as during operation with fuel, both natural gas and syngas (50% CO and 50% H_2). The operation with syngas is used to estimate the material's performance with solid fuels without using solid fuel in the experiment, as syngas is the intermediate formed during char gasification. The oxygen release behaviour of the material can be studied during fluidisation in inert atmosphere. Temperature, air flow and fuel flow have been varied during the experiments to evaluate their effect on the performance of the oxygen carriers. All experiments have been conducted during continuous operation for several hours. Two fluidised bed systems have been used, one designed for a fuel flow of 300 W and one designed for a fuel flow of 10 kW.

2.1. Oxygen-Carrier Materials

The oxygen carrier materials have been produced by spray drying at VITO in Belgium. The raw materials, most often metal oxides, are mixed with water and some organic additives and then sprayed in fine droplets into a hot chamber whereby the liquid evaporates and the raw materials form small particles. The material is then sintered at a high temperature for four hours. During this time the raw materials react to form the combined oxide structure and the material hardens. Usually a higher sintering temperature and a longer sintering time will give particles with higher mechanical stability, but with lower reactivity. The oxygen-carrier materials, the sintering temperature and particle properties are summarised in Table 1. These materials have all been examined in a laboratory batch reactor previously and have been chosen for continuous operation in larger reactor units due to their good characteristics. The oxygen carrier names reported in the table are identical with those used in the papers.

Table 1. Oxygen-carrier materials, sintering temperature and particle properties.

	Paper I	Paper II		Paper III			Paper IV	
Name	$CaMn_{0.9}Mg_{0.1}O_{3-\delta}$	$Fe_{0.66}Mn_{1.33}SiO_3$	$FeMnSiO_3$	F22M44-S33	F22M55-S22	F22M66-S11	MnSi	MnSiTi
Sintering temp. (°C)	1300	1100	1100	1200	1200	1200	1150	1140
Raw materials (wt%)	46.8% Mn_3O_4 50.5% $Ca(OH)_2$ 2.7% MgO	47.3% Mn_3O_4 27.9% SiO_2 24.8% Fe_2O_3	35.3% Mn_3O_4 27.8% SiO_2 36.9% Fe_2O_3	47.3% Mn_3O_4 27.9% SiO_2 24.8% Fe_2O_3	57.7% Mn_3O_4 18.1% SiO_2 24.2% Fe_2O_3	67.5% Mn_3O_4 8.9% SiO_2 23.6% Fe_2O_3	75% Mn_3O_4 25% SiO_2	66.7% Mn_3O_4 22.2% SiO_2 11.0% TiO_2
Mean size (μm)	137	153	147	153	145	139	136	126
Bulk density (kg/m^3)	1920	1026	1240	1030	1000	1470	1000	1688
Attrition index (wt%/h)	0.6	32.3	1.2	19.3	16.3	4.6	17.4	0.5

The bulk density reported was measured as the mass poured into a known volume. The attrition index reported was calculated from measurements using a customized jet cup; see the article by Rydén et. al. for a description of the jet cup and testing methodology. [37] The results from these tests with fresh material are used here as a comparison to the experimental attrition behaviour in the hot unit.

2.2. Experimental Setups

Two continuous chemical-looping reactor systems have been used in the study. They are described in the sections below.

2.2.1. 300 W Unit

The smaller unit is a circulating fluidised bed reactor designed for a thermal power of 300 W. The reactor consists of three compartments: the air reactor, the fuel reactor and the downcomer, which is also functioning as a loop seal. The reactor is depicted to the left in Figure 2 with the air reactor coloured blue, the fuel reactor coloured red and the upper loop seal coloured green. The lower loop seal cannot be seen in the figure and is located in the bottom of the system between the wind box of the air reactor and the wind box of the fuel reactor. To the right in Figure 2 the reactor is shown from a side view with the particle separation box at the gas outlet included.

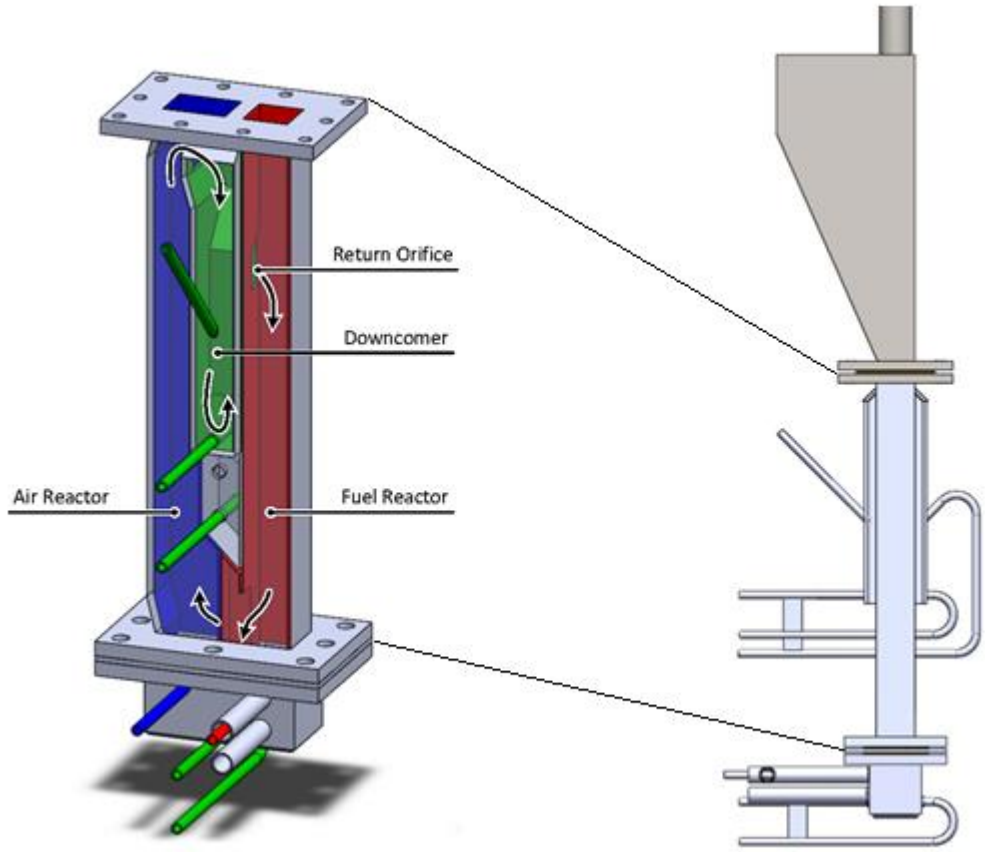

Figure 2. Schematic illustration of the smaller fluidised bed reactor: open front view to the left and side view including the particle separation box to the right.

The air reactor is divided into two parts with a lower bed section in which the cross section (40 x 25 mm) is larger than in the riser section above the bed (25 x 25 mm). The precondition for achieving solids circulation is a gas velocity in the air reactor high enough to carry the particles up from the bed surface. When the gas with the suspended particles exits the air reactor it enters a separation box where the gas velocity decreases due to an increased cross sectional area. This low-velocity section results in a separation of gas and particles, and the latter will fall down towards the air reactor. However, a certain fraction of particles enter the downcomer between the air and fuel reactor. The downcomer works as a J-type loop seal (25 x 25 mm) with an overflow exit into the fuel reactor. After fluidising in the fuel reactor the particles eventually return to the air reactor through the lower loop seal.

The air reactor is fluidised with air and the fuel reactor is fluidised with natural gas or syngas during fuel operation and with carbon dioxide during oxygen release experiments. Porous quartz plates are used as gas distributors in both the air reactor and the fuel reactor. The downcomer and the lower loop seal are fluidized with argon which is added through small holes in the pipes which can be seen in Figure 2. Since the reactor system has a high area to volume ratio, much

heat will be lost. Therefore the reactor system is enclosed in an electric furnace in order to keep the desired temperature.

The temperature is measured with one thermocouple in the air reactor and one in the fuel reactor. The thermocouples are located approximately 1 cm above the distributer plate in each reactor. The pressure drops in the reactor system are measured by pressure transducers in the air reactor, fuel reactor and in the downcomer. The pressure drops are measured in order to be able to assess the fluidization behaviour and the solids inventory in the different parts of the reactor system.

The outlet of the fuel reactor is connected to a water seal with a 1-2 cm column of water giving a slightly higher pressure in the fuel reactor than in the air reactor. A part of each outlet stream is led through a particle filter and a gas conditioning unit before entering the gas analysers.

2.2.2. 10 kW Unit

The larger unit is a 10 kW_{th} chemical-looping pilot plant for gaseous fuels. The reactor system consists of two interconnected fluidized beds, the air reactor and the fuel reactor. A schematic picture of the experimental setup can be seen in Figure 3.

The air reactor has an inner diameter of 150 mm. A riser is connected to the air reactor and it is the gas velocity through the air reactor and the riser which creates the driving force for the circulation. The separation of gas and particles is managed by a cyclone after the riser. The particles are brought from the cyclone to the fuel reactor through a downcomer and a loop seal. The latter assures that no gas will leak into or out of the fuel reactor. The fuel reactor consists of a bubbling fluidized bed which is fluidised by the gaseous fuel. The lower part of the fuel reactor has an inner diameter of 150 mm and the higher part has an inner diameter of 260 mm. Particles leave the fuel reactor via an overflow exit, and fall down into a second loop seal leading back into the air reactor. There is a vertical plate attached inside the fuel reactor which prevents particles entering the bed to by-pass the bed to the overflow exit. Thus, the solids flow will first go downwards on one side of this plate, turn and go upwards on the other side. The height from the bottom of the air reactor to the top of the riser is 2230 mm.

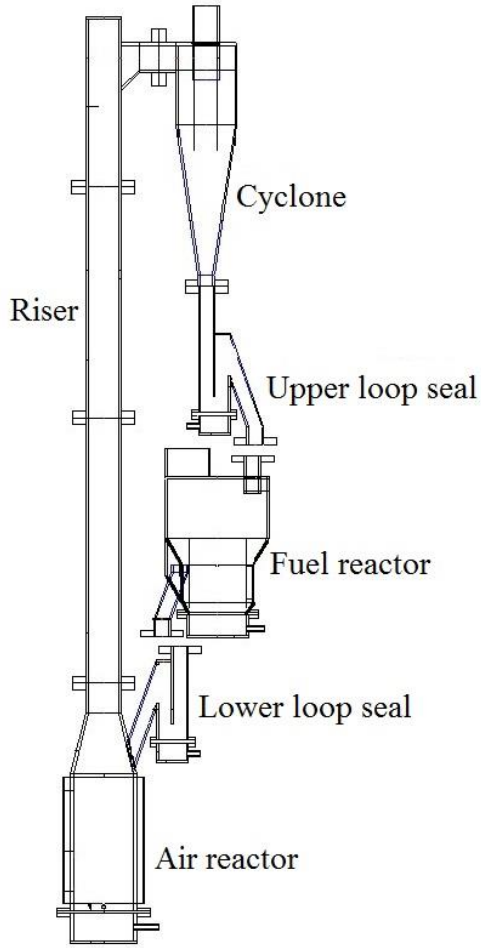

Figure 3. A schematic picture of the larger experimental setup.

The air reactor is fluidised by air preheated to 1000°C added through nozzles in the bottom plate and both loop seals are fluidized by nitrogen added through porous quartz plates. The nitrogen used to fluidise the particle seals escapes through both the air reactor and the fuel reactor and thus dilutes both exhaust gas streams. To avoid the nitrogen dilution, the particle seals can be fluidized by steam instead. This option was not utilised during these experiments.

The stream of exhaust gas leaving the cyclone is first led through finned pipes for passive cooling, then a part of the stream is led on to the gas conditioning system and the gas analysers, and the remaining gas is led through a bag filter. The exhaust gas stream from the fuel reactor is also led through finned pipes before a part of the stream is led to the gas conditioning system and the gas analysers, and the remaining gas passes a water seal, where the steam condensate is collected and elutriated particles are captured.

The temperature is measured with thermocouples at eight points in the reactor system, three in the air reactor, one in the riser, one in the cyclone, one in the higher loop seal and two in the fuel reactor. Pressure drops in the reactor systems are measured by 20 pressure transducers. The

pressure drops are measured in order to be able to assess the fluidisation behaviour and the particle inventory in different parts of the reactor system.

A supervision system is used to be able to operate the system during nights. If temperature or gas concentrations are not kept within certain accepted intervals, the supervision system will shut off the fuel flow to the fuel reactor and replace it with nitrogen.

One important difference between the 10 kW reactor and the 300 W reactor is the fluidisation velocities. In the 10 kW unit, the particles are exposed to velocities around 3 m/s in the riser and much higher velocities in the cyclone and around the nozzles of the bottom plate in the air reactor. These are velocities more similar to those found in commercial circulating fluidised bed boilers. To illustrate the conditions for the particles it can be noted that in previous operation the high velocities have created holes in both the bottom plate of the air reactor and in the cyclone. Thus the oxygen carrier particles are exposed to conditions more similar to those in an industrial unit. The velocities in the 300 W unit are considerably smaller, in the order of 0.7 m/s and there are no cyclones or nozzles creating harsh conditions for the particles. Another advantage with using the larger unit is that the overall mass balance of the particles and the attrition behaviour evaluation are more reliable. However, considerably more particles are needed to operate the 10 kW unit, around 10-20 kg, and thus experiments are only possible materials of which large amounts of particles are available.

2.3. Data Analysis

Both experimental reactor units are connected to identical gas conditioning systems and gas analysers. The gas analysers measure the concentration of carbon dioxide, carbon monoxide, methane and oxygen from the fuel reactor and the concentrations of oxygen and carbon dioxide from the air reactor. Methane, carbon monoxide and carbon dioxide are measured with IR-sensors while oxygen is measured with a paramagnetic sensor. Gas concentrations, temperatures and pressure drops are logged every ten seconds.

From the measurements the CO_2 yield was calculated to evaluate the combustion performance. The CO_2 yield is defined as the amount of carbon dioxide formed divided by the total amount of carbon species in the outlet flow according to:

$$\gamma_{CO_2} = \frac{x_{CO_2}}{x_{CO_2}+x_{CO}+x_{CH_4}} \qquad (5)$$

During the experiments in the smaller unit, the outlet from the fuel reactor is also analysed with a gas chromatograph which measures hydrogen and nitrogen, as well as the previously mentioned gases. The hydrogen measurements give additional information of the fuel conversion and are especially interesting for the conversion of syngas. The nitrogen measurements are used to measure the amount of air leakage from the air reactor to the fuel reactor. During some of the experiments the leakage was high enough to be accounted for in the data evaluation. The leakage occurred both ways and was detected by measuring carbon dioxide in the air reactor and nitrogen

in the fuel reactor. The carbon dioxide fraction in the air reactor does not interfere much with the data analysis. However, the air leakage to the fuel reactor affects the results both for oxygen release and combustion performance. The gas leakage has been located to the top of the reactor by injecting tracer gas in the pressure measurement taps. It was therefore assumed that the air which leaked into the fuel reactor had the same concentrations of oxygen and nitrogen as the outlet air from the air reactor. The fraction of oxygen leaking from the air reactor is quantified by the nitrogen concentration out of the fuel reactor and the oxygen concentration out of the air reactor:

$$x_{O_2,leakage} = x_{N_2,FR} \frac{x_{O_2,AR,out}}{x_{N_2,AR,out}} \tag{6}$$

In the same way the oxygen fraction related to the release of oxygen from the oxygen carrier particles is calculated as:

$$x_{O_2,released} = x_{O_2,FR} - x_{N_2,FR} \frac{x_{O_2,AR,out}}{x_{N_2,AR,out}} \tag{7}$$

The circulation rate in the larger unit has been assessed to evaluate the operating conditions in the system. The following expression, previously used by Linderholm et. al. [38] for this unit, has been used to calculate the net solid flux:

$$G_s = \rho_{exit}(u - u_t) = -\frac{1}{g}\frac{dp}{dh}(u - u_t) \tag{8}$$

The net solids flux calculated by this expression overestimates the actual circulation, but it is still a useful measure for comparing particle circulations. The net solid flux multiplied with the cross sectional area of the riser is referred to as circulation index (CI) and is expressed in kg/min.

3. Results

3.1. Operation with Calcium Manganite Perovskite (Paper I)

$CaMn_{0.9}Mg_{0.1}O_{3-\delta}$ was operated with natural gas in a chemical-looping unit designed for a fuel flow of 10 kW_{th}. During the last part of the heat up of the unit, the fuel reactor was fluidised with nitrogen and the oxygen release could be studied. The oxygen concentration in the exhaust gas from the fuel reactor during three heat-up periods with different air flows is shown in Figure 4. A higher air flow will give higher oxygen concentration in the air reactor and a higher circulation rate of oxygen-carrier particles. However, the air flow did not seem to influence the oxygen release significantly. The oxygen release increased with temperature and appears to level out at around 900°C.

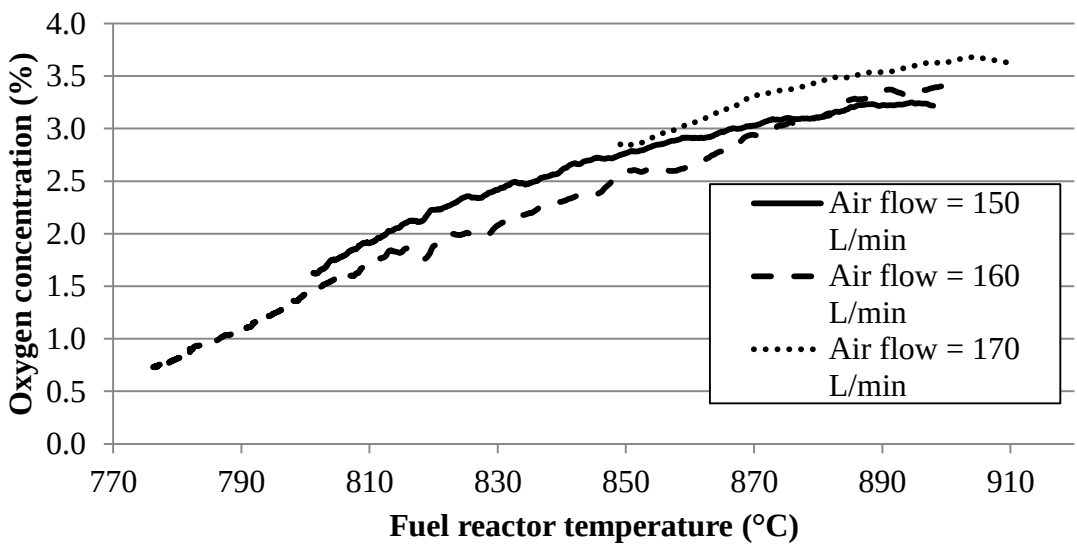

Figure 4. Oxygen concentration in the fuel reactor as a function of fuel reactor temperature during fluidisation with nitrogen in the fuel reactor.

The gas concentrations in the exhaust gas from the fuel reactor during fuel operation are shown in Figure 5. The air flow was kept constant and the temperature was kept within a rather small interval during this period. The fuel flow was varied and the effect is seen in the gas concentrations. The fuel was completely converted and excess oxygen released from the oxygen carrier was present during the periods with a fuel flow of 9 L_N/min. When the fuel flow was increased, the excess oxygen was consumed and the fuel conversion was no longer complete. Then the fuel flow was slightly decreased and the concentrations of methane and carbon monoxide decreased somewhat. When the fuel flow was decreased to 9 L_N/min again, full fuel conversion and excess oxygen was obtained once again. This showed that it is possible to obtain a desired gas outlet composition by only changing the fuel flow. Since a very pure stream of

carbon dioxide without oxygen, methane and carbon monoxide present is an advantage for gas storage, this result is very desirable.

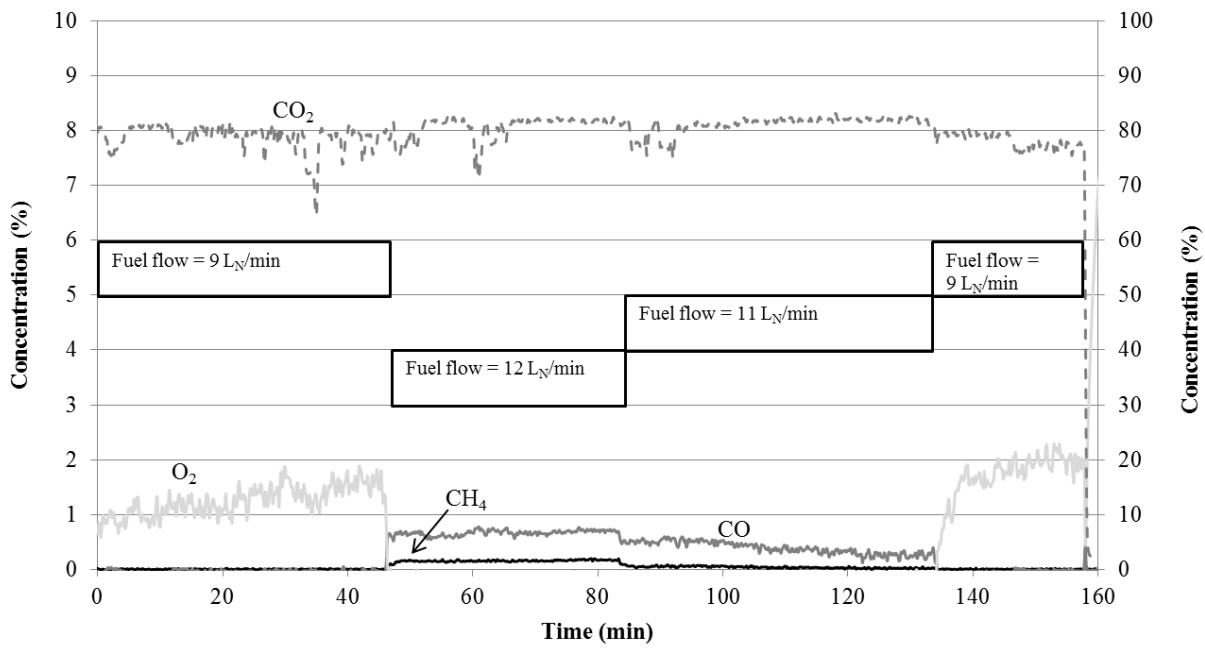

Figure 5. The gas concentrations at the outlet of the fuel reactor as a function of time with F_{ar} = 200 L_N/min, F_{fr} = 9-12 L_N/min (6.6-8.8 kW) and T_{fr} = 935-955ºC. Note that the concentration of CO_2 has a separate y-axis.

As previously mentioned, the air flow will affect the rate of solids circulation. The CO_2 yield as a function of circulation rate is shown in Figure 6. A rather distinct correlation between the solids circulation rate and the fuel conversion was observed.

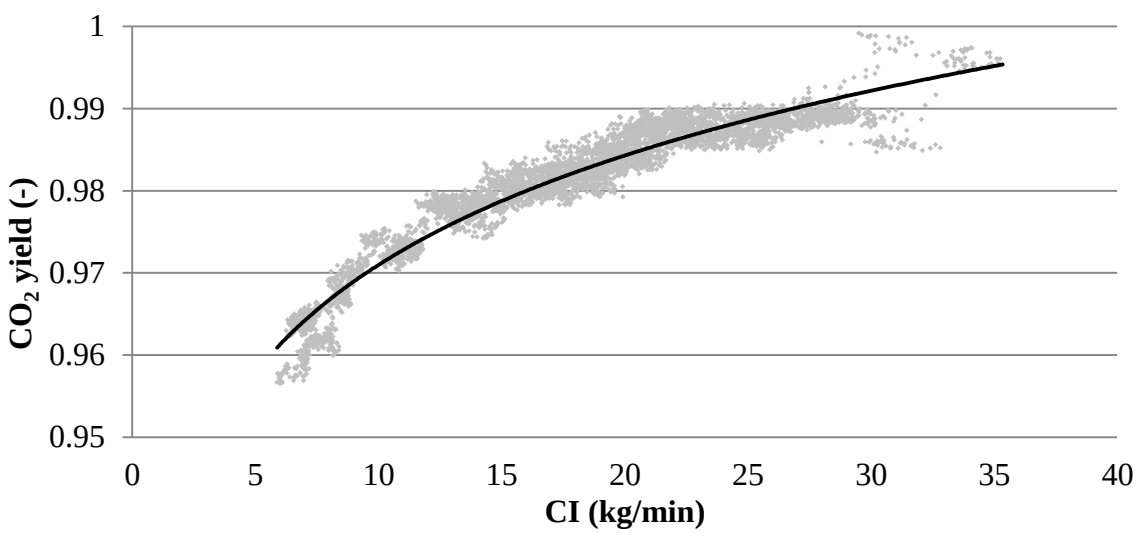

Figure 6. CO_2 yield as a function of circulation index with F_{ar} = 170 L_N/min and F_{fr} = 9 L_N/min at a fuel rector temperature of 930-950°C.

The oxygen carrier particles showed good fluidisation properties throughout the experiments and there was little evidence of particle attrition. Two samples of 300 g of the elutriated material were sieved after each filter emptying, normally after each day of operation, and the particle size distribution was noted. The mass fraction of fines, i.e. particles smaller than 45 µm, at each filter cleaning can be seen in Figure 7. The material loss during operation with fuel was typically 0.32 kg/h and the mass fraction of fines was 0-0.4% from the first fuel addition on day 5. The highest mass fraction of fines obtained with fuel addition, i.e. 0.4%, would mean a loss of fines of 0.0085 mass%/h, which corresponds to a lifetime of 12 000 h. It should be noted however that these numbers are indicative of a very low attrition, but that the exact numbers are uncertain due to a high elutriation rate combined with a low fraction of fines.

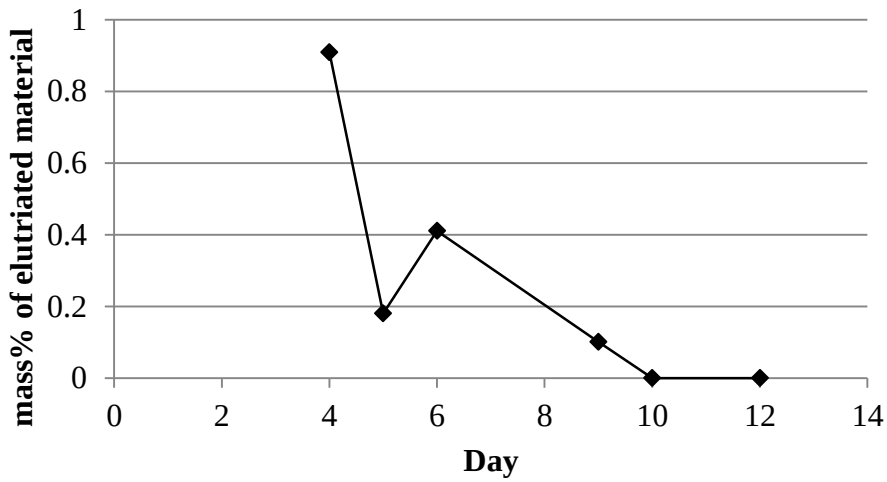

Figure 7. The average mass fraction of fines, <45µm, for the two sieved samples of elutriated material versus day of operation.

3.2. Phase Diagrams for Iron-Manganese-Silica Combined Oxides (Paper II and III)

The equilibrium solid phase of the combined oxide is decided by the temperature and the oxygen partial pressure. A phase diagram with a constant oxygen partial pressure and a varying temperature of combined oxides of manganese, iron and silica can be seen in Figure 8. The phase diagram has been calculated with the software FactSage 6.3 using the FToxid database. The oxygen partial pressure was set to 0.05 atm which would correspond to an expected outlet concentration of oxygen from the air reactor. The molar fraction of silica was set to 33%, which is the silica fraction of the examined oxygen carriers $FeMnSiO_3$ and $Fe_{0.66}Mn_{1.33}SiO_3$, which are marked in the diagram as solid vertical lines.

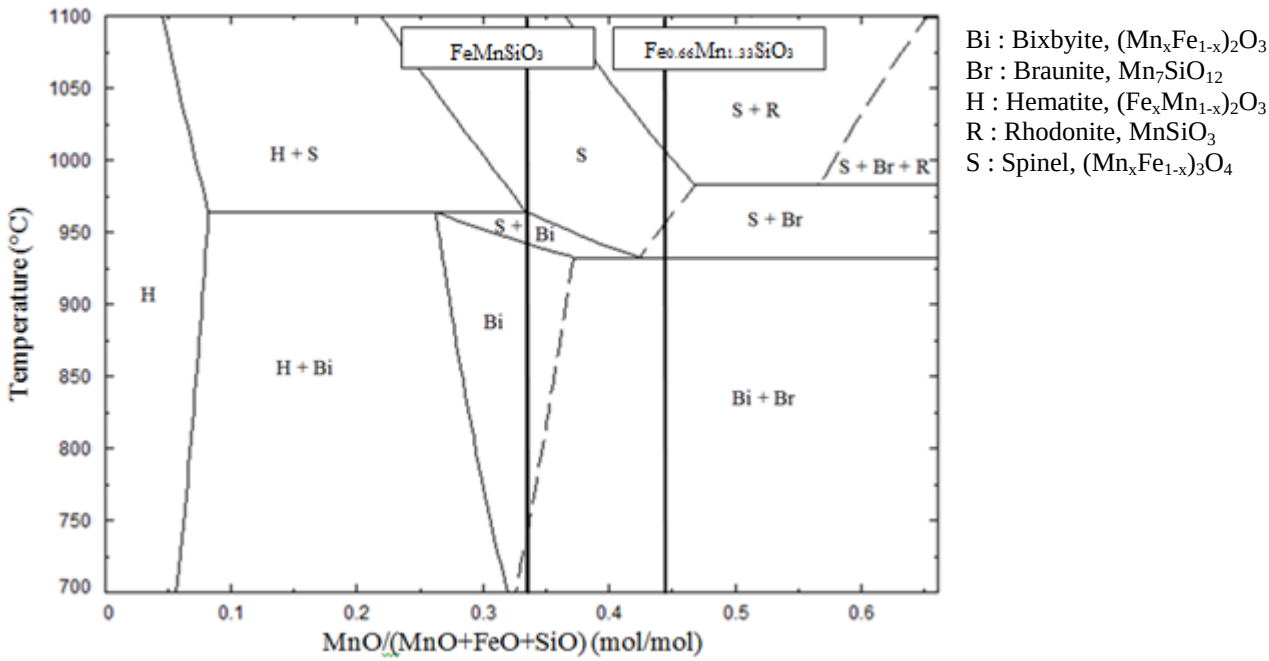

Figure 8. Phase diagram of MnO-FeO-SiO in an oxygen partial pressure of 0.05 atm. The molar fraction of silica is fixed at 33 mol%. Silica is also present as various forms of SiO_2, but these are not marked in the phase diagram. The vertical lines denote the composition of the oxygen carriers examined in this work.

The phase diagram calculated is consistent with the phase diagram of the manganese-iron systems [21, 39]. The dashed lines in the phase diagram represent the main effect of the presence of silica as it marks the transition to braunite. Braunite is the mineral name for Mn_7SiO_{12} with small impurities of other metals, but is used here for the pure phase. Another silica containing phase in this system is rhodonite consisting of $MnSiO_3$ with dilute amounts of $FeSiO_3$. Silica is also present as various forms of SiO_2, but these are not marked in the phase diagram. Both hematite and bixbyite are mixtures of Mn_2O_3 and Fe_2O_3, where Mn_2O_3 is the main component in bixbyite and Fe_2O_3 is the main component in hematite. The spinel marked in the diagram has the chemical formula $(Mn_xFe_{1-x})_3O_4$.

There are several reactions possible in the above system, of which some can release gas phase oxygen. The phase transitions which could be relevant for chemical-looping conditions can be seen in Table 2. These reactions could be induced either by a change in temperature or a change in oxygen partial pressure. A lower oxygen partial pressure lowers the temperature for the transition and a higher partial pressure of oxygen increases the temperature for the transition. According to Figure 8, the phase transition between bixbyite and spinel should be complete for $Fe_{0.66}Mn_{1.33}SiO_3$ at around 930°C, while for $FeMnSiO_3$ bixbyite is present up to 965°C.

It is also possible that the transition from braunite to rhodonite could be interesting for chemical-looping. This reaction would occur at around 980-1000°C and would only be relevant for oxygen carriers with a high content of manganese.

Table 2. The relevant phase transitions and the corresponding reaction formula.

Transition	Reaction
Bixbyite - Spinel	$6(Mn,Fe)_2O_3 \leftrightarrow 4(Mn,Fe)_3O_4 + O_2$
Braunite - Rhodonite	${}^{2}/_{3}\, Mn_7SiO_{12} + 4SiO_2 \leftrightarrow {}^{14}/_{3}\, MnSiO_3 + O_2$
Spinel/Rhodonite -Tephroite	$Mn_3O_4 + 3MnSiO_3 \leftrightarrow 3Mn_2SiO_4 + {}^{1}/_{2}\, O_2$

A similar phase diagram as presented in Figure 8 is shown in Figure 9 for the MnO-FeO-SiO system. However, here the oxygen partial pressure is shown as a function of manganese content at 900°C. This phase diagram has also been calculated with the software FactSage 6.3 using the FToxid database. The molar fraction of iron was set to 22 mol%, which is the iron fraction of F22M44S33, F22M55S22 and F22M66S11 materials investigated in this work, see Table 2. These compositions are marked in the diagram as solid vertical lines. It should be noted that F22M44S33 and $Fe_{0.66}Mn_{1.33}SiO_3$ have identical component composition. For the experimental evaluation however, it should be noted that these two materials have different sintering temperatures.

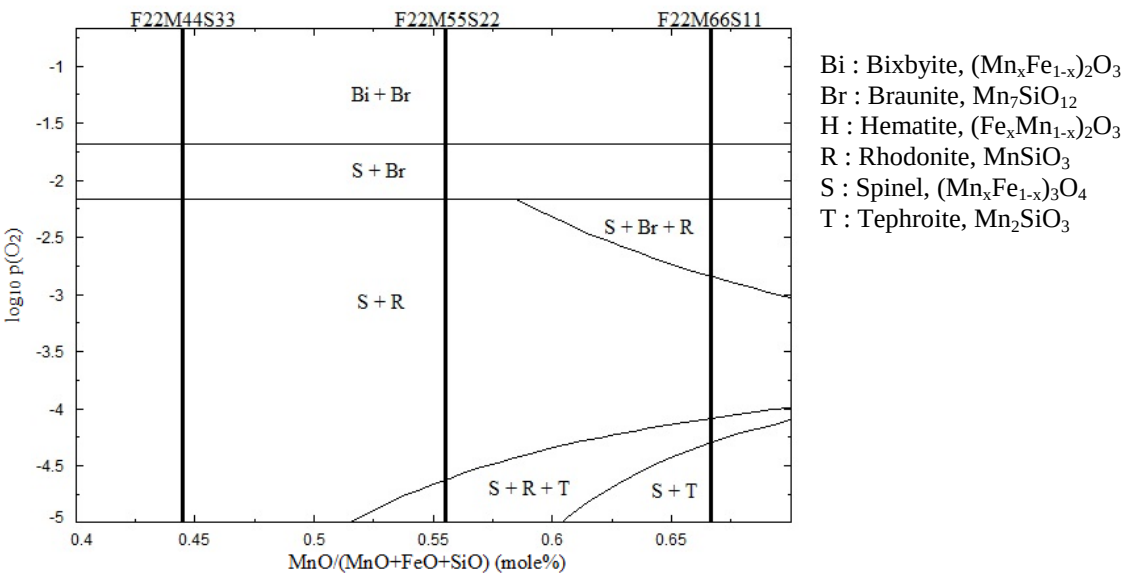

Figure 9. Phase diagram of MnO-FeO-SiO at 900°C and atmospheric pressure. The molar fraction of iron is fixed at 22%. Silica is also present as various forms of SiO_2, but these are not marked in the phase diagram. The vertical lines denote the composition of the oxygen carriers.

At higher temperatures, the phase transitions would occur at higher oxygen partial pressures. This implies that the surrounding oxygen concentration would not need to be as low to enable the phase transition to tephroite at higher temperatures. As can be seen in the phase diagram, F22M66S11 (and possibly also F22M55S22) has the potential to undergo all three phase transitions listed in Table 2 when circulating between the air reactor and the fuel reactor.

3.3. Operation with Iron-Manganese-Silica Combined Oxides (Paper II and III)

Five materials consisting of combined iron-manganese-silica oxides have been evaluated in the 300 W unit. The oxygen release for the materials sintered at 1100°C is shown in Figure 10. The materials showed very similar behaviour and the released oxygen concentration increased significantly above 900°C.

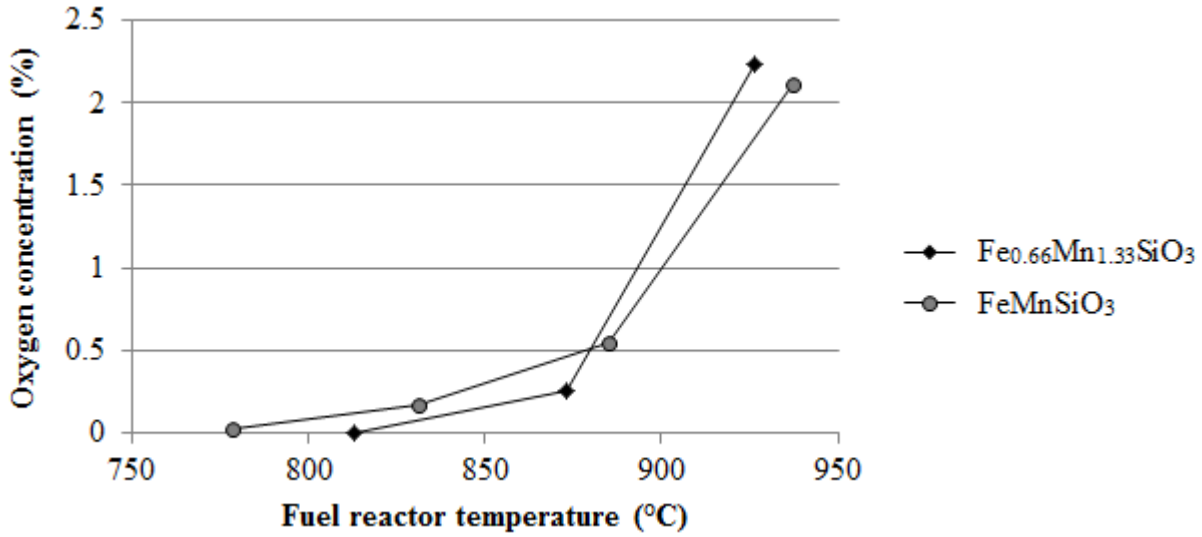

Figure 10. Oxygen release as a function of fuel reactor temperature during operation with $Fe_{0.66}Mn_{1.33}SiO_3$ and $FeMnSiO_3$.

The oxygen release for the materials sintered at 1200°C is shown in Figure 11. In this case the oxygen concentration is plotted as a function of time to show that the oxygen release was not constant at the highest temperature. A possible explanation for this behaviour could be that the residence time in the air reactor was insufficient for full reoxidation in the air reactor at this temperature. This is not unexpected since the oxygen equilibrium partial pressure increases with temperature which reduces the driving force for oxidation. However, the decrease in oxygen release was reversible and the same concentration could be reached again after full oxidation in air. These materials released higher concentrations of oxygen than the materials sintered at 1100°C in the temperature interval investigated.

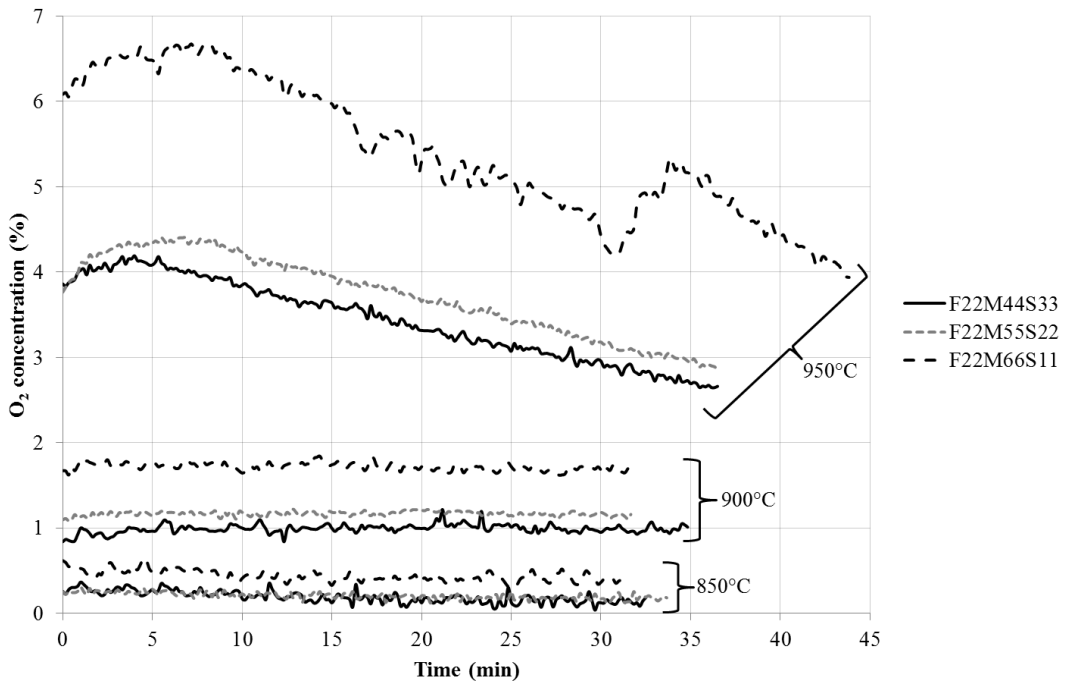

Figure 11. Measured oxygen concentration for each investigated temperature as a function of time during operation with F22M44S33, F22M55S22 and F22M66S11.

The fuel conversion during operation with natural gas for the iron-manganese-silica combined oxides is shown in Figure 12 and Figure 13. The figures show the calculated CO_2 yield as a function of fuel reactor temperature and the fuel reactor solids inventory used during each experiment. $Fe_{0.66}Mn_{1.33}SiO_3$ was the only material which fully converted the fuel even though this material was operated with one of the lowest solids inventories. In general the materials with the higher fractions of manganese performed better during fuel operation.

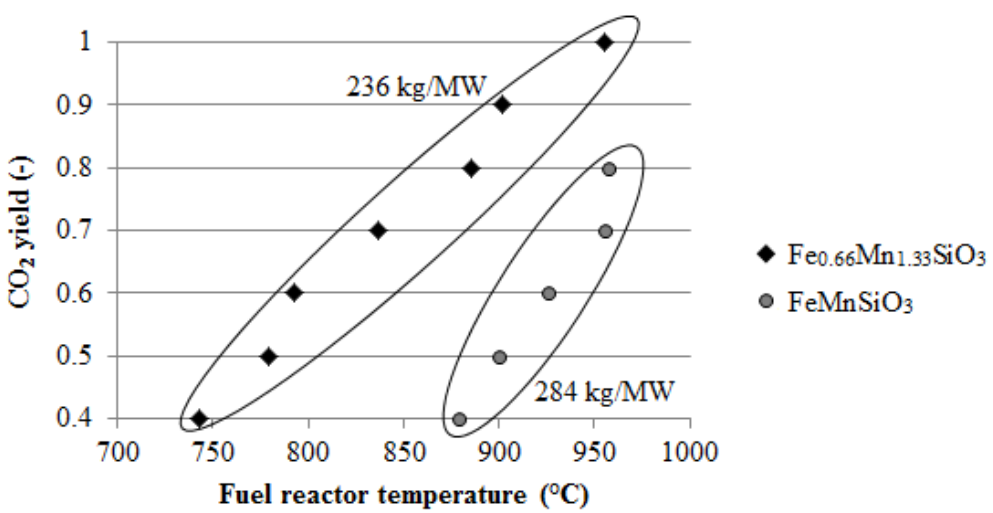

Figure 12. CO_2 yield as a function of fuel reactor temperature during natural gas operation with a fuel power of 220 W for $Fe_{0.66}Mn_{1.33}SiO_3$ and $FeMnSiO_3$.

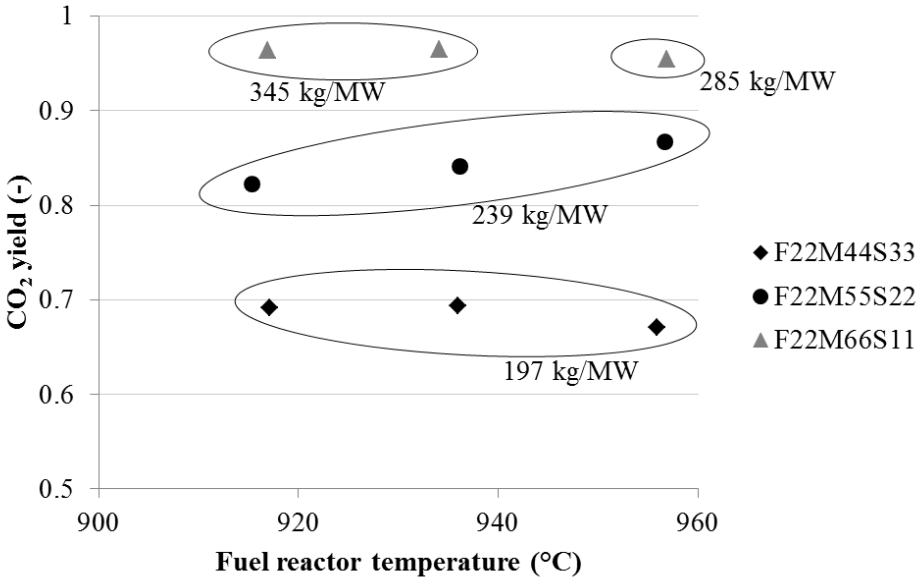

Figure 13. CO_2 yield as a function of fuel reactor temperature during natural gas operation with a fuel power of 220-290 W for F22M44S33, F22M55S22 and F22M66S11.

The same trend could be seen when the oxygen carrier materials were operated with syngas as fuel. During operation with $Fe_{0.66}Mn_{1.33}SiO_3$ and F22M66S11 the CO_2 yield was above 99% at temperatures above 800°C. The fuel conversion increased with temperature for all the investigated materials.

The operation with each material was continued until the solids circulation failed. This was caused by material attrition for all the iron-manganese-silica materials. The operational time with fuel addition can be used as a qualitative measure for the mechanical stability of the particles. The possible fuel operation time and the measured attrition indices are summarised in Table 3. The materials with a lower attrition index could be operated for a longer time with fuel addition.

Table 3. The possible operational time with fuel addition and the measured attrition index for the combined iron-manganese-silica oxygen carries.

Material	Operational time with fuel (h)	Attrition index (wt%/h)
$Fe_{0.66}Mn_{1.33}SiO_3$	8.2	32.3
$FeMnSiO_3$	16.1	1.2
F22M44S33	9.9	19.3
F22M55S22	10.8	16.3
F22M66S11	14.1	4.6

3.4. Operation with Manganese-Silica Combined Oxides (Paper IV)

The concentration of oxygen released during fluidisation in inert atmosphere with MnSiTi and MnSi is shown in Figure 14. In this case there was a larger difference in oxygen release between the materials than between the temperature levels in contrast to the iron-manganese-silica materials. The oxygen release is shown against time as the concentration continuously decreased at the higher temperature levels. This behaviour was most distinct for MnSiTi and this is in this case believed to be a result of the high density of this material. The oxygen release experiments were carried out with a lower air flow than the fuel operation and this has likely resulted in too low circulation for the heavier titania containing material. This was confirmed during later operation when the oxygen release was studied during a higher air flow, which gave a more constant released oxygen concentration. In general these materials released much lower concentrations of oxygen than the iron-manganese-silica materials did.

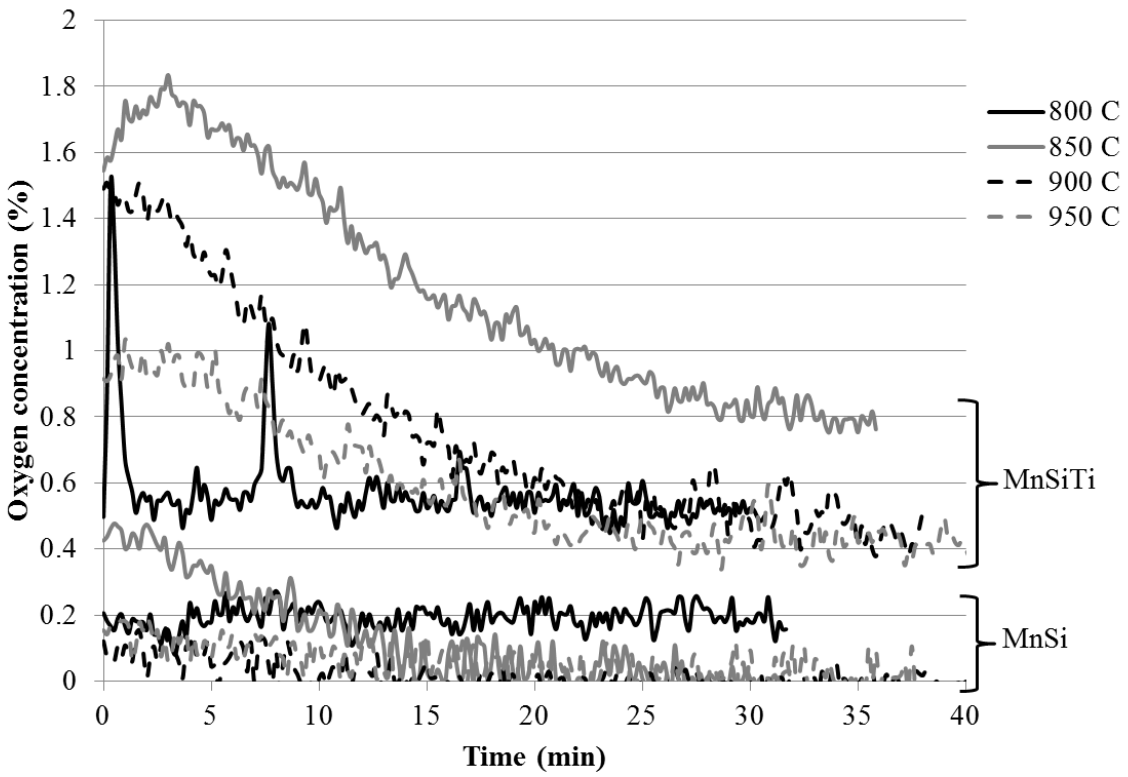

Figure 14. Released oxygen concentration for MnSiTi and MnSi during periods with constant temperature.

Even though MnSiTi released much higher concentration of oxygen than MnSi did, MnSi had a much higher fuel conversion both during operation with syngas and with natural gas. The CO_2 yield as a function of fuel reactor temperature during syngas combustion is shown in Figure 15. Full fuel conversion was reached at 950°C with MnSi even though the solids inventory in the fuel reactor was as low as 142 kg/MW. The fuel conversion increased with temperature for both materials.

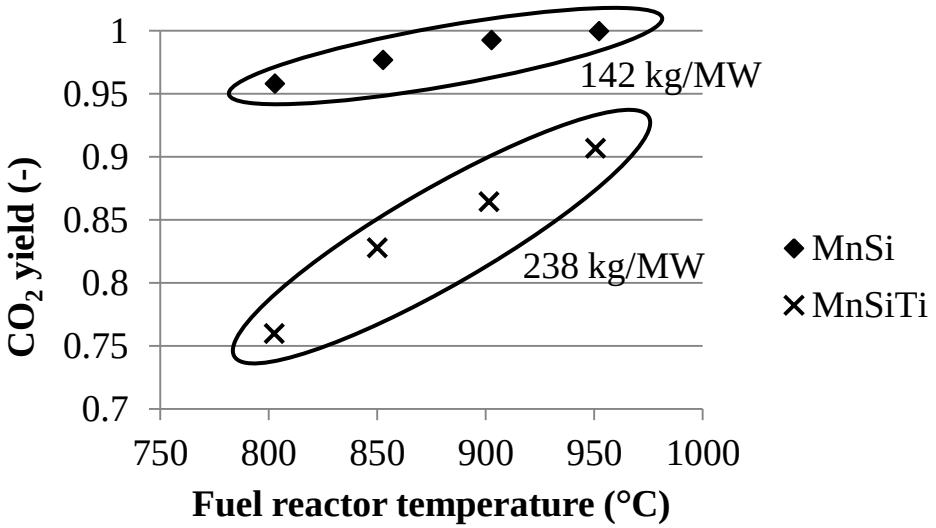

Figure 15. CO_2 yield as function of fuel reactor temperature during combustion of syngas with MnSiTi and MnSi. Each data point represents an average value during a period with constant temperature.

The same behaviour was observed during operation with natural gas as fuel; the fuel conversion increased with temperature for both materials and reached 100% with MnSi at 950°C. Figure 16 shows the CO_2 yield as a function of fuel reactor temperature during the operation with natural gas. The fuel conversion was much lower for natural gas than for syngas except at high temperature with MnSi where the results were comparable to the syngas operation.

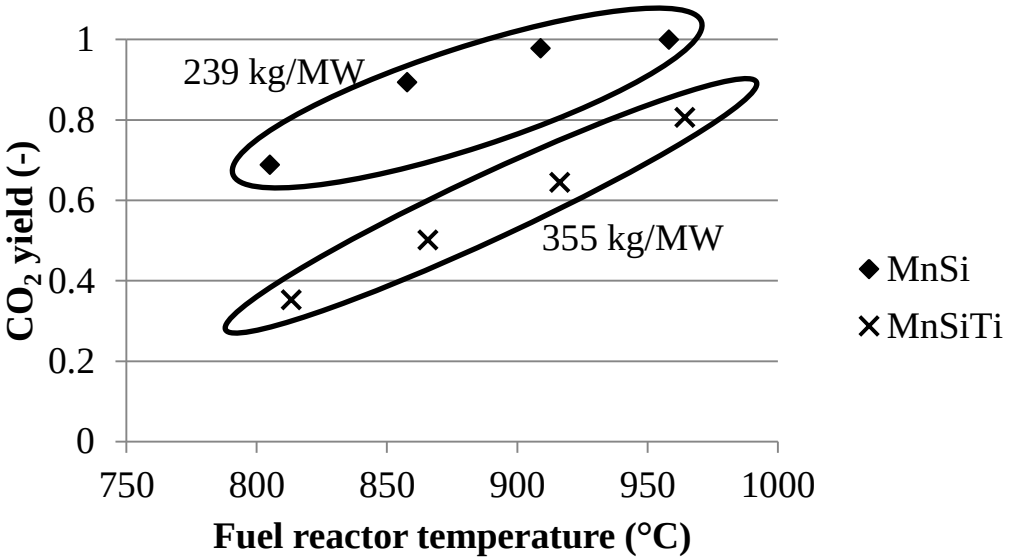

Figure 16. CO_2 yield as function of fuel reactor temperature during combustion of natural gas with MnSiTi and MnSi. Each data point represents an average value during a period with constant temperature.

The operation with MnSi had to be aborted after only seven hours with fuel addition. The reason was a high attrition rate and finally the circulation was disrupted by a too high fraction of very fine particles. Most of the particles were elutriated from the system and ended up in the filters, but even the material left in the reactor system was not possible to fluidise due to a high fraction of fines.

MnSiTi was operated for 24 h with fuel addition before the circulation was disrupted. It is not entirely clear why the operation encountered problems at this time. When the reactor system was opened, still almost 90% of the added mass remained in the system and did not contain any significant amount of fines. From this observation it is clear that the attrition rate was much lower than for MnSi. These observations correspond well with the measured attrition indices of the fresh materials.

4. Discussion

The materials investigated have shown very promising results and it is motivated to further investigate manganese combined oxides as oxygen carriers. Calcium manganite has proven to work very well in operation with gaseous fuels, but it is uncertain how this material would perform in long-term operation with sulphur containing fuels. Calcium manganites may be deactivated by the sulphur present in most solid fuels. [40] The formation and decomposition of solid sulphur compounds in conditions varying between oxidising and reducing are difficult to predict. Operational experience with solid fuels indicates that sulphur compounds are formed but the results are not conclusive. [41] However, it would need to be investigated more before calcium manganites are further developed for sulphur containing solid fuels.

The materials aiming for operation with solids fuels examined in this study, i.e. the materials based on manganese combined with iron and silica, show great promise, but need to be further improved before being investigated in a larger scale. Especially the combination of high reactivity with fuel and good mechanical stability is highly desirable. From the current investigation, it is quite clear that the mechanical stability can be improved. For example, an addition of a small amount of titania to an oxygen carrier of manganese and silica showed very positive effects on mechanical stability. Also the production process could likely be optimised to improve performance. Sintering temperature and time, milling method and raw powder particle size are some parameters which could be adjusted.

Oxygen carriers operated with solid fuels would also need to be rather cheap as it is presumed that the lifetime will be shortened due to fuel impurities and losses in separation of ash and oxygen carrier. At present it is not clear whether the added cost of manufacturing materials will be compensated for by longer lifetime and better performance. Therefore it is also relevant to investigate naturally occurring materials such as manganese ores. Iron and silica are common constituents of manganese ores, which also means that they may be similar to the synthesised oxygen carriers investigated in this study, so the results from this study are also relevant for a better understanding of the behaviour of manganese ore in chemical-looping combustion.

5. Conclusions

Manganese combined oxides have been shown to have interesting properties for chemical-looping with oxygen uncoupling (CLOU). At the start of this work only a limited number of experiments had been performed with these types of materials in continuous operation. In this work, eight oxygen carrier materials consisting of manganese combined oxides have been examined as oxygen carriers; seven materials in a 300 W unit and one material in a 10 kW unit. All materials investigated have been shown to work and all materials are able to release oxygen, although several materials showed poor mechanical stability. The main conclusions to draw from these experiments are:

- The manganese perovskite material works very well in continuous operation with a low rate of attrition. The material is able to fully convert the fuel at relevant temperature levels.
- Combined oxides of iron, manganese and silica showed good performance in operation. It is possible to reach full conversion of the fuel and the investigated materials with the highest content of manganese had the highest fuel conversion. However, the mechanical stability of the particles needs to be improved.
- Combined oxides of manganese and silica also showed good performance. It is possible to reach full fuel conversion and it is possible to produce particles with significantly improved mechanical stability by adding titanium to the material. The addition of titania, however, lowered the gas conversion. The possibility to get good mechanical stability without compromising with the reactivity of the material needs to be further investigated.

References

[1] IPCC. Climate Change 2013 The Physical Science Basis Working Group I Contribution to the Fifth Assessment Report of the Intergovernmental Panel on Climate Change. In: Stocker T, Qin D, Plattner G, Tignor M, Allen S, Boschung J, et al., editors. Cambridge, United Kingdom and New York, USA 2013.

[2] Parmesan C, Yohe G. A globally coherent fingerprint of climate change impacts across natural systems. Nature. 2003;421:37-42.

[3] IPCC. Climate Change 2014: Mitigation of Climate Change. Contribution of Working Group III to the Fifth Assessment Report of the Intergovernmental Panel on Climate Change. In: Edenhofer O, Pichs-Madruga R, Sokona Y, Farahani E, Kadner S, Seyboth K, et al., editors. Cambridge, United Kingdom and New York, USA 2014.

[4] IPCC. IPCC Special Report on Carbon Dioxide Capture and Storage. In: Metz B, Davidson O, de Coninck H, Loos M, Meyer L, editors. Cambridge, United Kingdom2005.

[5] Boot-Handford ME, Abanades JC, Anthony EJ, Blunt MJ, Brandani S, Mac Dowell N, et al. Carbon capture and storage update. Energy Environ Sci. 2014;7:130-89.

[6] Mattisson T, Lyngfelt A, Leion H. Chemical-looping with oxygen uncoupling for combustion of solid fuels. International Journal of Greenhouse Gas Control. 2009;3:11-9.

[7] Lewis WK, Gilliland ER. Production of pure carbon dioxide. In: patent U, editor. USA 1954.

[8] Ishida M, Jin H. A novel combustor based on chemical-looping reactions and its reaction kinetics. Journal of Chemical Engineering of Japan. 1994;27:296-301.

[9] Lyngfelt A, Thunman H. Chapter 36 - Construction and 100 h of Operational Experience of A 10-kW Chemical-Looping Combustor. Carbon Dioxide Capture for Storage in Deep Geologic Formations. Amsterdam: Elsevier Science; 2005. p. 625-45.

[10] Lyngfelt A. Oxygen Carriers for Chemical Looping Combustion - 4 000 h of Operational Experience. Oil & Gas Science and Technology. 2011;66:2.

[11] Adanez J, Abad A, Garcia-Labiano F, Gayan P, de Diego LF. Progress in Chemical-Looping Combustion and Reforming technologies. Progress in Energy and Combustion Science. 2012;38:215-82.

[12] Jerndal E, Mattisson T, Lyngfelt A. Thermal Analysis of Chemical-Looping Combustion. Chemical Engineering Research and Design. 2006;84:795-806.

[13] Linderholm C, Mattisson T, Lyngfelt A. Long-term integrity testing of spray-dried particles in a 10-kW chemical-looping combustor using natural gas as fuel. Fuel. 2009;88:2083-96.

[14] Pröll T, Kolbitsch P, Bolhàr-Nordenkampf J, Hofbauer H. A novel dual circulating fluidized bed system for chemical looping processes. AIChE Journal. 2009;55:3255-66.

[15] Lyngfelt A, Mattisson T. Materials for chemical-looping combustion. Power Engineering for CCS Power Plants: WILEY-VCH Verlag; 2011.

[16] Abad A, Mattisson T, Lyngfelt A, Johansson M. The use of iron oxide as oxygen carrier in a chemical-looping reactor. Fuel. 2007;86:1021-35.

[17] Abad A, Adánez-Rubio I, Gayán P, García-Labiano F, de Diego LF, Adánez J. Demonstration of chemical-looping with oxygen uncoupling (CLOU) process in a 1.5 kWth continuously operating unit using a Cu-based oxygen-carrier. International Journal of Greenhouse Gas Control. 2012;6:189-200.

[18] Rydén M, Jing D, Källén M, Leion H, Lyngfelt A, Mattisson T. CuO-based oxygen-carrier particles for chemical-looping with oxygen uncoupling - Experiments in batch reactor and in continuous operation. Industrial and Engineering Chemistry Research. 2014;53:6255-67.

[19] Rydén M, Leion H, Mattisson T, Lyngfelt A. Combined oxides as oxygen-carrier material for chemical-looping with oxygen uncoupling. Applied Energy. 2013;113:1924-32.

[20] Shulman A, Cleverstam E, Mattisson T, Lyngfelt A. Manganese/Iron, Manganese/Nickel, and Manganese/Silicon Oxides Used in Chemical-Looping With Oxygen Uncoupling (CLOU) for Combustion of Methane. Energy & Fuels. 2009;23:5269-75.

[21] Azimi G, Leion H, Rydén M, Mattisson T, Lyngfelt A. Investigation of different Mn-Fe oxides as oxygen carrier for chemical-looping with oxygen uncoupling (CLOU). Energy and Fuels. 2013;27:367-77.

[22] Jing D, Arjmand M, Mattisson T, Rydén M, Snijkers F, Leion H, et al. Examination of oxygen uncoupling behaviour and reactivity towards methane for manganese silicate oxygen carriers in chemical-looping combustion. International Journal of Greenhouse Gas Control. 2014;29:70-81.

[23] Mattisson T, Jing D, Azimi G, Rydén M, Van Noyen J, Lyngfelt A. Using $(Mn_xFe_{1-x})_2SiO_5$ as oxygen carriers for chemical-looping with oxygen uncoupling (CLOU). Presented at AIChE Annual Meeting November 3-8, San Fransisco 2013.

[24] Rydén M, Lyngfelt A, Mattisson T. Combined manganese/iron oxides as oxygen carrier for chemical looping combustion with oxygen uncoupling (CLOU) in a circulating fluidized bed reactor system. Energy Procedia. 2011;4:341-8.

[25] Leonidova EI, Leonidov IA, Patrakeev MV, Kozhevnikov VL. Oxygen non-stoichiometry, high-temperature properties, and phase diagram of $CaMnO_{3-\delta}$. Journal of Solid State Electrochemistry. 2011;15:1071-5.

[26] Leion H, Larring Y, Bakken E, Bredesen R, Mattisson T, Lyngfelt A. Use of $CaMn_{0.875}Ti_{0.125}O_3$ as oxygen carrier in chemical-looping with oxygen uncoupling. Energy and Fuels. 2009;23:5276-83.

[27] Hallberg P, Jing D, Rydén M, Mattisson T, Lyngfelt A. Chemical looping combustion and chemical looping with oxygen uncoupling experiments in a batch reactor using spray-dried $CaMn_{1-x}M_xO_{3-\delta}$ (M = Ti, Fe, Mg) particles as oxygen carriers. Energy and Fuels. 2013;27:1473-81.

[28] Rydén M, Lyngfelt A, Mattisson T. $CaMn_{0.875}Ti_{0.125}O_3$ as oxygen carrier for chemical-looping combustion with oxygen uncoupling (CLOU)—Experiments in a continuously operating fluidized-bed reactor system. International Journal of Greenhouse Gas Control. 2011;5:356-66.

[29] Hallberg P, Källén M, Jing D, Snijkers F, Van Noyen J, Rydén M, et al. Experimental investigation of $CaMnO_{3-\delta}$ based oxygen carriers used in continuous chemical-looping combustion. Int J Chem Eng. 2014;2014.

[30] Lyngfelt A. Chemical-looping combustion of solid fuels - Status of development. Applied Energy. 2014;113:1869-73.

[31] Markström P, Lyngfelt A, Linderholm C. Chemical-Looping Combustion in a 100 kW Unit for Solid Fuels. 21st International Conference on Fluidized Bed Combustion. Naples 2012.

[32] Pröll T, Mayer K, Bolhàr-Nordenkampf J, Kolbitsch P, Mattisson T, Lyngfelt A, et al. Natural minerals as oxygen carriers for chemical looping combustion in a dual circulating fluidized bed system. 9th International Conference on Greenhouse Gas Control Technologies, GHGT-9. 1 ed. Washington DC2009. p. 27-34.

[33] Cuadrat A, Abad A, García-Labiano F, Gayán P, de Diego LF, Adánez J. The use of ilmenite as oxygen-carrier in a $500W_{th}$ Chemical-Looping Coal Combustion unit. International Journal of Greenhouse Gas Control. 2011;5:1630-42.

[34] Arjmand M, Leion H, Mattisson T, Lyngfelt A. Investigation of different manganese ores as oxygen carriers in chemical-looping combustion (CLC) for solid fuels. Applied Energy. 2014;113:1883-94.

[35] Linderholm C, Lyngfelt A, Cuadrat A, Jerndal E. Chemical-looping combustion of solid fuels – Operation in a 10 kW unit with two fuels, above-bed and in-bed fuel feed and two oxygen carriers, manganese ore and ilmenite. Fuel. 2012.

[36] Mendiara T, Abad A, de Diego LF, García-Labiano F, Gayán P, Adánez J. Biomass combustion in a CLC system using an iron ore as an oxygen carrier. International Journal of Greenhouse Gas Control. 2013;19:322-30.

[37] Rydén M, Moldenhauer P, Lindqvist S, Mattisson T, Lyngfelt A. Measuring attrition resistance of oxygen carrier particles for chemical looping combustion with a customized jet cup. Powder Technology. 2014;256:75-86.

[38] Linderholm C, Abad A, Mattisson T, Lyngfelt A. 160 h of chemical-looping combustion in a 10 kW reactor system with a NiO-based oxygen carrier. International Journal of Greenhouse Gas Control. 2008;2:520-30.

[39] Kjellqvist L, Selleby M. Thermodynamic assessment of the Fe-Mn-O system. Journal of Phase Equilibria and Diffusion. 2010;31:113-34.

[40] Arjmand M, Kooiman RF, Rydén M, Leion H, Mattisson T, Lyngfelt A. Sulfur tolerance of $Ca_xMn_{1-y}M_yO_{3-\delta}$ (M = Mg, Ti) perovskite-type oxygen carriers in chemical-looping with oxygen uncoupling (CLOU). Energy and Fuels. 2014;28:1312-24.

[41] Schmitz M, Linderholm C, Lyngfelt A. Chemical Looping Combustion of Sulphurous Solid Fuels using Spray-Dried Calcium Manganate Particles as Oxygen Carrier. 12th International Conference on Greenhouse Gas Technologies. Austin, USA 2014.